Localized deep levels in $Al_xGa_{1-x}N$ epitaxial films with various Al compositions*

Shi Li-Yang(时俪洋)[a], Shen Bo(沈 波)[a]†, Yan Jian-Chang(闫建昌)[b], Wang Jun-Xi(王军喜)[b], and Wang Ping(王 平)[a]

[a] State Key Laboratory of Artificial Microstructure and Mesoscopic Physics, School of Physics, Peking University, Beijing 100871, China
[b] R&D Center for Semiconductor Lighting, Institute of Semiconductors, Chinese Academy of Sciences, Beijing 100083, China

(Received 11 April 2014; revised manuscript received 27 May 2014; published online 24 September 2014)

By using high-temperature deep-level transient spectroscopy (HT-DLTS) and other electrical measurement techniques, localized deep levels in n-type $Al_xGa_{1-x}N$ epitaxial films with various Al compositions ($x = 0$, 0.14, 0.24, 0.33, and 0.43) have been investigated. It is found that there are three distinct deep levels in $Al_xGa_{1-x}N$ films, whose level position with respect to the conduction band increases as Al composition increases. The dominant defect level with the activation energy deeper than 1.0 eV below the conduction band closely follows the Fermi level stabilization energy, indicating that its origin may be related to the defect complex, including the anti-site defects and divacancies in $Al_xGa_{1-x}N$ films.

Keywords: localized deep levels, current–voltage, capacitance–voltage, high-temperature deep-level transient spectroscopy techniques

PACS: 61.66.Dk, 61.72.–y, 61.72.J–, 61.72.jd **DOI:** 10.1088/1674-1056/23/11/116102

1. Introduction

$Al_xGa_{1-x}N$ epitaxial films, particularly Al-rich $Al_xGa_{1-x}N$ films, are attractive for their applications in UV light-emitting diodes (LED), UV-detectors, and high-power electronic devices.[1–3] However, it is known that the external quantum efficiency of $Al_xGa_{1-x}N$-based LEDs is limited to within several percent, and $Al_xGa_{1-x}N$/GaN-based transistors suffer from drain current instability and lack long-term reliability.[3] It has been considered that these phenomena have a strong connection with deep-level defects in $Al_xGa_{1-x}N$.[4] In order to improve and optimize device performance, it is necessary to study the localized centers and understand their influence on the electrical properties of $Al_xGa_{1-x}N$ alloys.

Moreover, up to now, few papers about the electrical characterization of localized deep levels in $Al_xGa_{1-x}N$ have been published, although photoluminescence (PL) or cathodoluminescene (CL) investigation had shown some characterization luminescence peaks related to the deep levels in $Al_xGa_{1-x}N$ and AlN.[5–8] In addition, such electrical characterization has been carried out on $Al_xGa_{1-x}N$ with an Al composition lower than 0.25,[3,9] presumably because of the difficulty in growing a thick $Al_xGa_{1-x}N$ layer with high Al composition of high quality. However, such studies are expected to provide information essential for the improvement and optimization of devices based on $Al_xGa_{1-x}N$ epitaxial films and quantum structures.

In this study, we report a detailed characterization of localized deep levels in Si-doped $Al_xGa_{1-x}N$ epitaxial thin films with various Al compositions, which are grown by means of metal–organic chemical vapor deposition (MOCVD), using high-temperature deep-level transient spectroscopy (HT-DLTS), as well as normal current–voltage (I–V) and capacitance–voltage (C–V) measuring techniques. Since $Al_xGa_{1-x}N$ alloys have an extremely wide band gap ranging from 3.4 eV to 6.2 eV, in order to detect deep levels with the activation energy larger than 1.0 eV, the measurement temperature range should extend to 600–800 K in standard DLTS measurements.[10] In our HT-DLTS system, the measuring temperature range can reach 77 K–800 K.

2. Experiments

The samples used in this study were grown on c-plane sapphire substrate by means of MOCVD and consisted of 250-nm Si-doped $Al_xGa_{1-x}N$ films with x in the range of 0, 0.14, 0.24, 0.33, and 0.43, respectively. After the initial nitridation step of sapphire substrate, a high-temperature AlN buffer layer with about 1-μm thickness was deposited. The n-type carrier concentration of the five samples was determined to be in the range of 10^{17} cm^{-3} by means of C–V measurements.

The thickness of the $Al_xGa_{1-x}N$ films was confirmed by a cross-sectional scanning electron microscope (SEM-Nova Nano SEM 430). The Al composition was determined using high-resolution X-ray diffraction (XRD-Bruker D8 discover). The crystal quality of AlGaN layer was also investigated by X-ray diffraction rocking curves (XRCs). For I–V, C–V, and DLTS measurements, circular Schottky diodes

*Project supported by the National Basic Research Program of China (Grant No. 2012CB619300) and the National Natural Science Foundation of China (Grant Nos. 11174008 and 61361166007).

†Corresponding author. E-mail: bshen@pku.edu.cn

© 2014 Chinese Physical Society and IOP Publishing Ltd

with 300-μm diameter were fabricated using the conventional photolithographic lift-off technique. The Ohmic contacts were formed using electron-beam deposition of Ti/Al/Ni/Au (30/175/35/100 nm), with subsequent annealing at 850 °C for 35 s in a nitrogen atmosphere, using a rapid thermal annealing system. The Schottky contacts were formed using electron-beam deposition of Ni/Au (50/150 nm). The dimensional layouts of fabricated Schottky diodes in the cross-sectional and top view are shown schematically in Fig. 1.

To characterize the fabricated devices, *I–V* and *C–V* characteristics were measured using an Agilent 4155C semiconductor parameter analyzer and a 4294A precision impedance analyzer at 1 MHz, respectively, at room temperature in the dark. DLTS measurements in a temperature range from 77 K to 800 K were carried out using the highly sensitivity $[10^{-7}(N_D - N_A) < N_T < 10^{-5}(N_D - N_A)]$ Semilab DS-83D system. During the DLTS measurements, the reverse bias was set at 2 V and periodically pulsed to 1 V for trap filling.

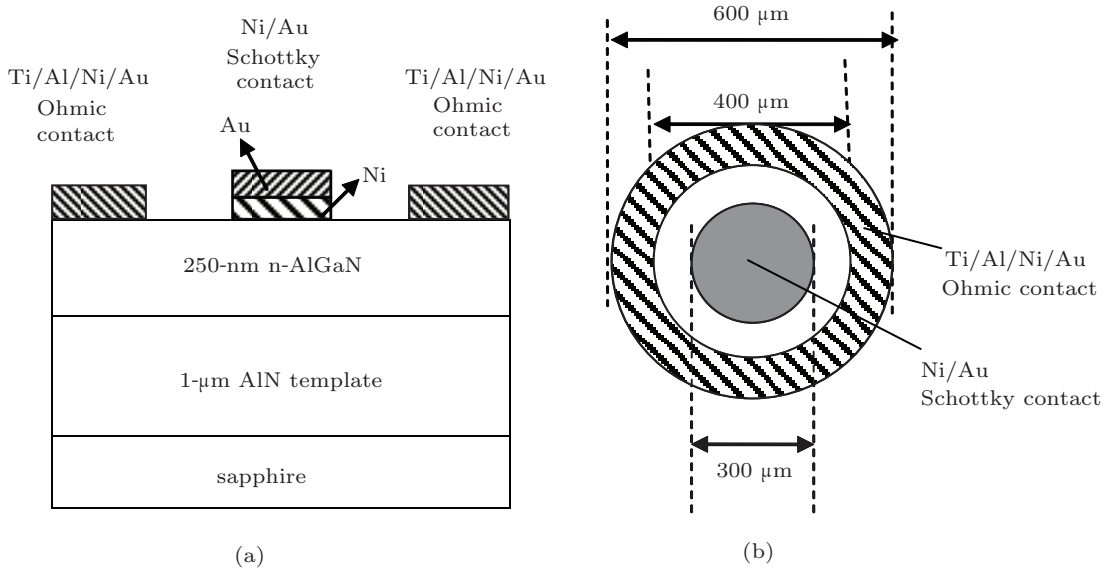


Fig. 1. Dimensional layout of fabricated Schottky diode in cross-sectional (a) and top view (b).

3. Results and discussion

Figure 2 shows typical measured *I–V* curves of the $Al_xGa_{1-x}N$ Schottky diodes with four different x values (x = 0.14, 0.23, 0.33, and 0.43).

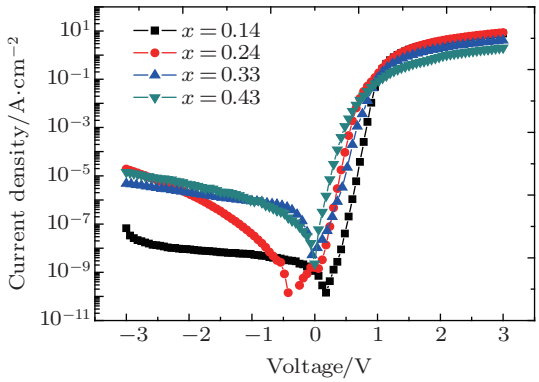


Fig. 2. (color online) *I–V* characteristics of the $Al_xGa_{1-x}N$ Schottky diodes with different Al compositions.

The experimental *I–V* characteristics were analyzed using the following equations:[11]

$$I = I_s\left[\exp\left(\frac{qV}{nkT}\right) - 1\right], \tag{1}$$

$$I_s = AA^*\exp\left(-\frac{\phi_B}{kT}\right), \tag{2}$$

where I_s is the saturation current density, q is the magnitude of electronic charge, k is the Boltzmann constant, ϕ_B is the barrier height, n is the ideality factor, A is the area of Schottky barrier contact, and A^* is the effective Richardson constant. The theoretical value of the effective Richardson constant is given by $A^* = 2\pi qm^*k^2/h^3$, where h is the Plank constant and m^* is the electron effective mass for AlGaN. Apparently, there have not been any reported experimental results of the electron effective mass in the literature, we estimated m^* for $Al_xGa_{1-x}N$ with different x by a linear interpolation from the theoretical value of $m^* = 0.35m_0$ for AlN and $m^* = 0.22m_0$ for GaN. The values of n obtained from Eqs. (1) and (2) are 1.56, 1.58, 1.82, and 1.85, respectively. The higher value of the ideality factor is greater than one due to the presence of interface states between the metal and the semiconductor because an interfacial film of atomic dimensions always exists between the metal and semiconductor, causing surface state assisted tunneling or leakage current.[12] In Fig. 2, the reverse bias leakage current density was generally very small and was below the order of 5×10^{-5} A/cm^2 at a reverse bias of 2 V in all of the samples studied.

The measured A^2/C^2 as a function of the applied voltage V for the Schottky diode samples is shown in Fig. 3. In general, the C–V relation for the Schottky diodes is[13]

$$\frac{A^2}{C^2} = \frac{2\,(V_{\rm bi} - V - kT/q)}{qN_{\rm d}\varepsilon_{\rm g}}, \tag{3}$$

where A is the area of the Schottky barrier contact, $V_{\rm bi}$ is the built-in potential, $N_{\rm d}$ is the carrier concentration, and $\varepsilon_{\rm g}$ is the dielectric constant of the $Al_xGa_{1-x}N$. The Schottky barrier height $\phi_{\rm B}$ is related to the $V_{\rm bi}$ by the relationship

$$\phi_{\rm B} = qV_{\rm bi} + qV_n, \tag{4}$$

where $V_n = (kT/q)\ln(N_{\rm c}/N_{\rm d})$ is the potential difference between the conduction band and the Fermi level of the n-type $Al_xGa_{1-x}N$. The $N_{\rm c}$ is the effective density of states in the conduction band of n-type AlGaN. The Schottky barrier height $\phi_{\rm B}$ for the $Al_xGa_{1-x}N$ alloys with x values of 0.14, 0.23, 0.33 and 0.43 is 1.25, 1.39, 1.41, and 1.61 eV, respectively. The detailed study of the surface state characterization of the $Al_xGa_{1-x}N$ samples will be described elsewhere.[14]

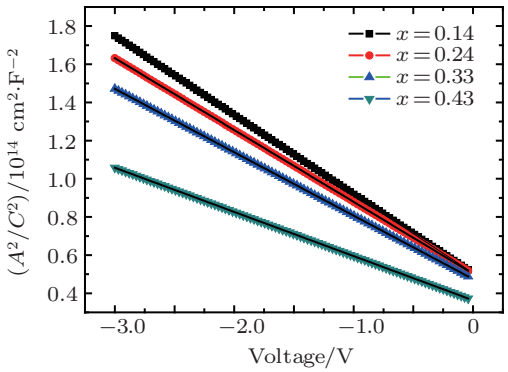


Fig. 3. A^2/C^2–V plot of the $Al_xGa_{1-x}N$ samples.

Si is the most widely used n-type dopant in an AlGaN ternary system. However, the contribution of these donors to the free carrier concentration for such a large band gap and in the presence of deep impurities is still unknown. For n-GaN, the Si donor level has been established to be approximately 20 meV.[9]

To determine the Si donor activation energy in AlGaN alloys, variable temperature Hall measurements were performed. As is shown in Fig. 4, the Si donor levels were obtained at approximately 33, 40, 50, and 57 meV, respectively, as x value increasing from 0.14, 0.23, 0.33 to 0.43, which indicates that Si remains a shallow donor in $Al_xGa_{1-x}N$ with Al composition x lower than 0.43. That is to say, in the following discussion about deep levels, we can ignore the effects of Si donors. The Si donor binding energy increases as x increases, which happens because of the smaller dielectric constant of AlN than GaN and the large effective mass of the electron in AlN.[15]

Figure 4 presents the DLTS spectra of $Al_xGa_{1-x}N$ samples with various x values. The emission rate windows in these spectra were 100 Hz and 200 Hz, respectively. The reverse bias up to 2 V restricts the depletion width to the $Al_xGa_{1-x}N$ layer during DLTS measurements. In order to compare the origin of deep-level defects in the $Al_xGa_{1-x}N$ alloys, a GaN sample was chosen as a reference. As shown in Fig. 4, three deep levels, which were labeled as E_{10}, E_{20}, and E_{30}, were clearly observed for GaN. These three deep levels are consistent with the activation energy range from 0.14 eV–0.27 eV (E_1),[16–19] 0.44 eV–0.62 eV (E_2),[16–21] and 0.67 eV–0.89 eV (E_3),[17,18] respectively, as observed by many groups. These defect levels are most likely associated with the point defects, such as N vacancy,[16,21,22] N anti-site,[18,22] and N interstitial,[18,23] respectively. However, Cho *et al.*[20] reported that the E_1 trap is related to the threading dislocation with $E_{\rm t} = 0.19$–0.23 eV and $\sigma_{\rm T} = 10^{-16}$–$10^{-15}$ cm^2. From these points of view, the origins of these levels are so far still unclear. The defect levels are denoted as E_{1i}, E_{2i}, and E_{3i} where $i = 1$, 2, 3, and 4 for our $Al_xGa_{1-x}N$ samples. With Al composition increasing, the DLTS signals of the three deep levels shift toward higher temperatures, which is similar to the defect levels in undoped $Al_xGa_{1-x}N$, as observed in photocurrent measurements.[24] In our study, the energy levels of E_{1i}, E_{2i}, and E_{3i} ($i = 1$, 2, 3, and 4) are from 0.27 eV, 0.39 eV, 0.49 eV to 0.53 eV, 0.48 eV, 0.59 eV, 0.75 eV to 0.81 eV, and 1.02 eV, 1.07 eV, 1.12 eV to 1.22 eV, respectively.

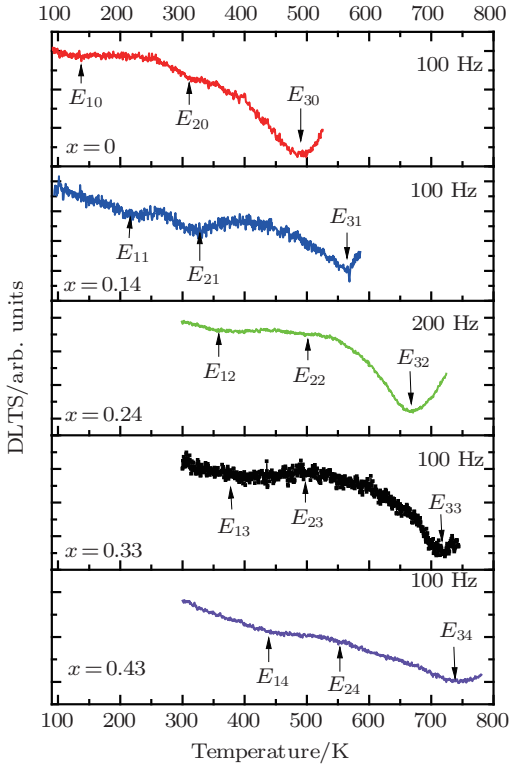


Fig. 4. (color online) The DLTS spectra of the $Al_xGa_{1-x}N$ Schottky diode samples with various Al compositions ranging from 0, 0.14, 0.24, 0.33, to 0.43 with the frequencies of 100 Hz and 200 Hz, respectively.

To extract more detailed information from the DLTS signals, the activation energy (ΔE) and capture cross section (σ_T) were obtained from Arrhenius plots, which were plotted from DLTS signals at different rate windows. Figure 5 presents the Arrhenius plots as a function of $\ln(e_n/T^2)$ versus $1000/T$, where e_n is the thermal emission rate of the electrons from deep state. The other parameters of the deep-level defects detected are summarized in Table 1.

Table 1. The DLTS parameters for the deep-level defects E_{1i}, E_{2i}, and E_{3i} ($i = 0$, 1, 2, 3, and 4) in Si-doped $Al_xGa_{1-x}N$ samples (x means Al composition; ΔE means activation energy; σ means capture cross-section; and, N_T means defect density).

x	E_{1i}	ΔE/eV	σ/cm^2	N_T/cm^{-3}	E_{2i}	ΔE/eV	σ/cm^2	N_T/cm^{-3}	E_{3i}	ΔE/eV	σ/cm^2	N_T/cm^{-3}
0	E_{10}	0.16	3.9×10^{-18}	7.7×10^{13}	E_{20}	0.45	1.2×10^{-17}	1.4×10^{14}	E_{30}	0.75	7.2×10^{-17}	2.1×10^{14}
0.14	E_{11}	0.27	4.4×10^{-19}	3.3×10^{14}	E_{21}	0.48	2.8×10^{-17}	4.2×10^{14}	E_{31}	1.02	2.3×10^{-17}	8.6×10^{14}
0.24	E_{12}	0.39	3.4×10^{-19}	6.3×10^{14}	E_{22}	0.59	3.4×10^{-18}	7.9×10^{14}	E_{32}	1.07	5.7×10^{-17}	2.0×10^{15}
0.33	E_{13}	0.49	4.1×10^{-19}	2.8×10^{14}	E_{23}	0.75	1.1×10^{-18}	3.3×10^{14}	E_{33}	1.12	4.4×10^{-17}	4.6×10^{14}
0.43	E_{14}	0.53	1.0×10^{-18}	1.2×10^{15}	E_{24}	0.81	5.8×10^{-17}	2.1×10^{15}	E_{34}	1.22	8.0×10^{-16}	2.3×10^{15}

By comparing the E_{10}, E_{20}, and E_{30} defects of n-GaN, we believe that the origins of three deep levels observed in the $Al_xGa_{1-x}N$ samples correspond to the same kinds of defects in GaN, respectively. From the Arrhenius plot obtained from different rate windows, the values of σ_T are almost constant at $\sim10^{-19}$ cm^2 for the E_{1i}, $\sim10^{-18}$ cm^2 for the E_{2i} and $\sim10^{-17}$ cm^2 for the E_{3i} ($i = 1$, 2, 3, and 4), respectively. As Al composition increasing, the extend defects, such as dislocations, are dominant rather than the point defects. As shown in Table 1, as Al composition increases, the E_T for the E_{1i}, E_{2i}, and E_{3i} ($i = 1$, 2, 3, and 4) levels becomes deeper. However, based on the AlGaN energy band gap, the values of the σ_T are in the order of $\sim 10^{-19}$ cm^2, $\sim10^{-18}$ cm^2, and $\sim10^{-17}$ cm^2, which implies the same origin for E_{1i}, E_{2i}, and E_{3i} ($i = 1$, 2, 3, and 4), respectively.

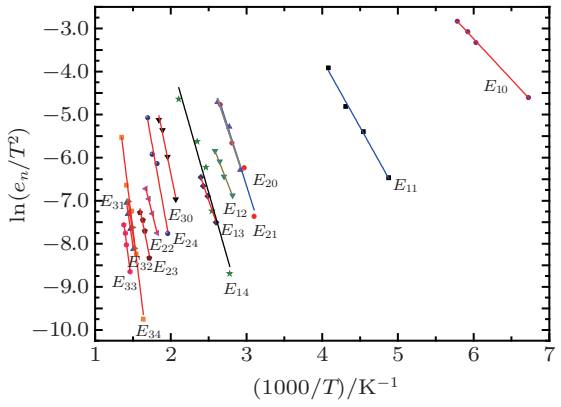


Fig. 5. (color online) The Arrhenius plots of the electron emission rates for the E_{1i}, E_{2i}, and E_{3i} ($i = 0$, 1, 2, 3, and 4) deep-defect levels.

To further gain insight into the physical origins of dominant deep level E_{3i} detected in the $Al_xGa_{1-x}N$, their energy positions are plotted in Fig. 6 as a function of the Al composition. The energy position was referred to the maximum of the valence band. Figure 6 also includes the DLTS data of dominant deep levels reported for GaN,[25–27] $Al_{0.12}Ga_{0.88}N$,[28] and $Al_{0.17}Ga_{0.83}N$.[29] For AlN, we plotted the deep-level emission energies in CL spectra.[30] To plot the conduction band edge E_c, reported band data, which were determined by optical observation,[31] cathodoluminescence[32] and photoreflectance measurements at room temperature,[33] were used as a function of the Al composition. As shown in Fig. 6, there is a tendency whereby the energy position of the dominant deep level E_{3i} approaches the midgap as the Al composition increases. Kimihito *et al.*[10] once observed two dominant deep levels with activation energies higher than 1.0 eV in $Al_xGa_{1-x}N$ with $x = 0.25$ and 0.37. To further investigate the behavior of the dominant level E_{3i}, the experimental data are referred to the Fermi level stabilization energy, E_{FS}, calculated by Walukiewicz *et al.*,[34] as indicated by the broken line in Fig. 6. Unexpectedly, the energy position of E_{3i} follows the E_{FS} trace well. On the basis of an amphoteric native defect model, Walukiewicz proposed the Fermi level stabilization energy as a pinning energy level in GaAs.[35] First principles calculations predict that the formation energies of simple defects (vacancies, interstitials and anti-site defects) in III–V semiconductors strongly depend on the Fermi level position.[36,37]

Figure 6 indicates the possibility that the origin of the E_{3i} is related to amphoteric native defects or their complex. In GaN, for example, the formation energies of V_{Ga} and V_N become equal when Fermi level approaches E_{FS}.[38] In this case, interactive defect transformation ($V_{Ga} + N_N \leftrightarrow N_{Ga} + V_N$ or $V_N + Ga_{Ga} \leftrightarrow Ga_N + V_{Ga}$) can create a defect complex, including anti-site defects and divacancies ($N_{Ga} + V_N + V_{Ga}$ or $Ga_N + V_{Ga} + V_N$). In AlGaN with high Al compositions, the formation energy of V_{Al} is much lower than that of V_{Ga}[30] leading to the E_{FS} position near the midgap, as shown in Fig. 6. In addition, it is likely that V_{Al} can play a leading part in the interactive defect transformation. In such a case, the origin of the dominant deep levels E_{3i} in high Al composition AlGaN is related to a complex consisting of ($N_{Al} + V_{Al} + V_N$) or ($Al_N + V_{Al} + V_N$).

On the other hand, Onuma *et al.*[39] and Uedeono *et al.*[30] pointed out that the complex defects consisting of

cation vacancies and oxygen (V_{III}–O_X) could create deep levels in $Al_xGa_{1-x}N$ alloys. A vacancy trapping mechanism for carbon–vacancy complex formation showing that C atoms are easily trapped in the vicinity of vacancy was also proposed.[40] Therefore, the oxygen-related or C-related complex point defects maybe the origin of deep levels E_{3i} in $Al_xGa_{1-x}N$ alloys observed in our study.

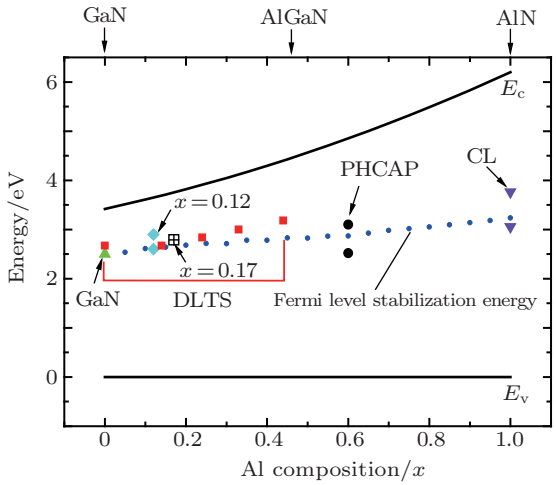


Fig. 6. (color online) Energy positions of the dominant deep levels E_{3i} ($i = 0$, 1, 2, 3, and 4) detected in $Al_xGa_{1-x}N$ samples (red square) as a function of Al compositions. Other symbols show data from Refs. [25]–[30]. The broken line indicates the Fermi level stabilization energy.

4. Conclusions

The localized deep levels in n-type $Al_xGa_{1-x}N$ epitaxial thin films with various Al compositions have been investigated by means of HT-DLTS and other electrical measurement techniques. The deep levels with the activation energies of E_{31}, E_{32}, E_{33}, and E_{34} of 1.02, 1.07, 1.12, and 1.22 eV, respectively, have been observed in $Al_xGa_{1-x}N$ films with $x = 0.14$, 0.24, 0.33, and 0.43. The energy positions of the E_{31}, E_{32}, E_{33}, and E_{34} in the $Al_xGa_{1-x}N$ closely follow the Fermi level stabilization energy on the basis of the amphoteric defect model, indicating that the possible origin of the E_{3i} is the defect complex, including anti-site defects and divacancies in $Al_xGa_{1-x}N$ films.

References

[1] Morkoc H, Strite S, Gao G B, Lin M E, Sverdlov B and Burns M 1994 *J. Appl. Phys.* **76** 1363
[2] Rumyantsev S L, Pala N, Shur M S, Gaska R, Levinshtein M E, Adivarahan V, Yang J, Simin G and Asif K M 2001 *Appl. Phys. Lett.* **79** 866
[3] Park Y S, Park C J, Park C M, Na J H, Oh J S, Yoon I T, Cho H Y, Kang T W and Oh J E 2005 *Appl. Phys. Lett.* **86** 152109
[4] Özdemir A F, Turut A and Kokce A 2003 *Thin Solid Films* **425** 210
[5] Nam K B, Nakarmi M L, Lin J Y and Jiang H X 2005 *Appl. Phys. Lett.* **86** 222108
[6] Nepal N, Nakarmi M L, Lin J Y and Jiang H X 2006 *Appl. Phys. Lett.* **89** 092107
[7] Sun Q, Wang H, Jiang D S, Jin R Q, Huang Y, Zhang S M, Yang H, Jahn U and Ploog K H 2006 *J. Appl. Phys.* **100** 123101
[8] Arehart A R, Allerman A A and Ringel S A 2011 *J. Appl. Phys.* **109** 114506
[9] Götz W, Johnson N M, Bremser M D and Davis R F 1996 *Appl. Phys. Lett.* **69** 2379
[10] Ooyama K, Sugawara K, Okuzaki S, Taketomi H, Miyake H, Hiramatsu K and Hashizume T 2010 *Jpn. J. Appl. Phys.* **49** 101001
[11] Qiao D, Yu L S, Lau S S, Redwing J M, Lin J Y and Jiang H X 2000 *J. Appl. Phys.* **87** 801
[12] Hashizume T, Kotani J and Hasegawa H 2004 *Appl. Phys. Lett.* **84** 4884
[13] Meneghini M, Bertin M, Stocco A, Santo G D, Marcon D, Malinowski P E, Chini A, Meneghesso G and Zanoni E 2013 *Appl. Phys. Lett.* **102** 163501
[14] Shi L Y, Shen B, Lu L W, Yan J C, Wang J X and Wang P 2014 *Chin. Phys. B* (In Press)
[15] Hwang J, Schaff W J, Eastman L F, Bradley S T, Brillson L J, Look D C, Wu J, Walukiewicz W, Furis M and Cartwright A N 2002 *Appl. Phys. Lett.* **81** 5192
[16] Götz W, Johnson N M, Amano H and Akasaki I 1994 *Appl. Phys. Lett.* **65** 463
[17] Hacke P, Detchprohm T, Hiramatsu K, Sawaki N, Tadatomo K and Miyake K 1994 *J. Appl. Phys.* **76** 304
[18] Haase D, Schmid M, Kuürner W, Dörnen A, Härle V, Scholz F, Burkard M and Schweizer H 1996 *Appl. Phys. Lett.* **69** 2525
[19] Lee W I, Huang T C, Guo J D and Feng M S 1995 *Appl. Phys. Lett.* **67** 1721
[20] Cho H K, Kim K S, Hong C H and Lee H J 2001 *J. Cryst. Growth* **223** 38
[21] Fang Z Q, Hemsky J W, Look D C and Mack M P 1998 *Appl. Phys. Lett.* **72** 448
[22] Chen S, Honda U, Shibata T, Matsumura T, Tokuda Y, Ishikawa K, Hori M, Ueda H, Uesugi T and Kachi T 2012 *J. Appl. Phys.* **112** 053513
[23] Fang Z Q, Look D C, Jasinski J, Benamara M, Weber Z L and Molnar R J 2001 *Appl. Phys. Lett.* **78** 332
[24] Polyakov A Y, Smirnov N B, Govorkov N V and Redwing J M 1998 *Solid-Sate Electron.* **42** 831
[25] Muret P, Philippe A, Monroy E, Munoz E, Beaumont B, Omnes F and Gibart P 2001 *Mater. Sci. Eng. B* **82** 91
[26] Ito T, Yoshikawa M and Egawa T 2008 *Phys. Stat. Solid C* **5** 2998
[27] Fang Z Q, Look D C, Kim D H and Adesida I 2005 *Appl. Phys. Lett.* **87** 182115
[28] Götz W, Johnson N M, Bremser M D and Davis R F 1996 *Appl. Phys. Lett.* **69** 2379
[29] Osaka J, Ohno Y, Kishimoto S, Maezawa K and Hizutani T 2005 *Appl. Phys. Lett.* **87** 222112
[30] Uedono A, Ishibashi S, Keller S, Moe C, Cantu P, Katona T M, Kamber D S, Wu Y, Letts E, Newman S A, Nakamura S, Speck J S, Mishra U K, DenBaars S P, Onuma T and Chichibu S F 2009 *J. Appl. Phys.* **105** 054501
[31] Bruner D, Angerer H, Bustarret E, Freudenberg F, Dimitrov R, Amabacher O and Stutzmann M 1997 *J. Appl. Phys.* **82** 5090
[32] Nikishin S A, Faleev N N, Zubrilov A S, Antipov V G and Temkin H 2000 *Appl. Phys. Lett.* **76** 3028
[33] Holtz M, Prokofyeva T, Seon M, Copeland K, Vanbuskirk J, Willians S, Nikishin S A, Tretyakov V, and Temkin H 2001 *J. Appl. Phys.* **89** 7977
[34] Walukiewicz W, Li S X, Wu J, Yu K M, Ager III J M, Haller E E, Lu H and Schaff W J 2004 *J. Cryst. Gowth* **269** 119
[35] Walukiewicz W 1987 *J. Vac. Sci. Technol. B* **5** 1062
[36] Walukiewicz W 1988 *J. Vac. Sci. Technol. B* **6** 1257
[37] Janotti A and van de Wall C G 2005 *Appl. Phys. Lett.* **87** 122102
[38] Walle C G V, Stampfl C and Neugebauer J 1998 *J. Cryst.Growth* **189–190** 505
[39] Onuma T, Chichibu S F, Uedono A, Sota T, Cantu P, Katona T M, Keading J F, Keller S, Mishra U K, Nakamura S and Denbarrs S P 2004 *J. Appl. Phys.* **95** 2495
[40] Zhou H B and Jin S 2013 *Chin. Phys. B* **22** 076104